The tunnel magnetoresistance in chains of quantum dots weakly coupled to external leads

2010 J. Phys.: Condens. Matter 22 015301

(http://iopscience.iop.org/0953-8984/22/1/015301)

J. Phys.: Condens. Matter **22** (2010) 015301 (11pp) doi:10.1088/0953-8984/22/1/015301

The tunnel magnetoresistance in chains of quantum dots weakly coupled to external leads

Ireneusz Weymann

Physics Department, Arnold Sommerfeld Center for Theoretical Physics, and Center for NanoScience, Ludwig-Maximilians-Universität, Theresienstrasse 37, D-80333 Munich, Germany
and
Department of Physics, Adam Mickiewicz University, Umultowska 85, 61-614 Poznań, Poland

E-mail: weymann@amu.edu.pl

Received 16 September 2009, in final form 30 October 2009
Published 8 December 2009
Online at stacks.iop.org/JPhysCM/22/015301

Abstract
We analyze numerically the spin-dependent transport through coherent chains of three coupled quantum dots weakly connected to external magnetic leads. In particular, using the diagrammatic technique on the Keldysh contour, we calculate the conductance, shot noise and tunnel magnetoresistance (TMR) in the sequential and cotunneling regimes. We show that transport characteristics greatly depend on the strength of the interdot Coulomb correlations, which determines the spatial distribution of the electron wavefunction in the chain. When the correlations are relatively strong, depending on the transport regime, we find both negative TMR as well as TMR enhanced above the Julliere value, accompanied with negative differential conductance (NDC) and super-Poissonian shot noise. This nontrivial behavior of tunnel magnetoresistance is associated with selection rules that govern tunneling processes and various high-spin states of the chain that are relevant for transport. For weak interdot correlations, on the other hand, the TMR is always positive and not larger than the Julliere TMR, although super-Poissonian shot noise and NDC can still be observed.

(Some figures in this article are in colour only in the electronic version)

1. Introduction

Tunnel magnetoresistance (TMR) measures changes in systems' transport properties when the magnetic configuration of the device switches from parallel to antiparallel alignment [1]. The tunneling current is usually larger in the parallel configuration, when transport occurs between the majority–majority and minority–minority spin bands, than in the antiparallel configuration, where electrons tunnel between majority and minority spin bands, which gives rise to the positive TMR effect. The TMR has been analyzed in various systems, including single-electron transistors and quantum dots [2–16]. In fact, a great deal of theoretical and experimental investigation has been devoted to spin-polarized transport through quantum dot structures. This is because quantum dots coupled to ferromagnetic leads are ideal candidates to study the fundamental interactions between spins and charges [17–20]. Furthermore, such systems are also being considered for applications in future spintronic devices as well as for quantum computing [21]. However, most of the existing theoretical considerations of spin-dependent transport in quantum dots involved only single- and double-dot systems [3–16], while experiments were carried out mainly for single-dot structures [22–31]. In particular, it has been shown [7] that the TMR in quantum dots weakly coupled to ferromagnetic leads is generally smaller than the value given by the Julliere model [1], $\mathrm{TMR}^{\mathrm{Jull}} = 2p^2/(1-p^2)$, where p is the spin polarization of the leads, which is characteristic of tunneling through a single tunnel junction. This result is rather intuitive, as by embedding a quantum dot structure between ferromagnetic electrodes, the tunneling processes through the system become incoherent due to spin–flip processes and spin relaxation in the dot, leading to suppressed TMR. Because the magnitude of the TMR is generally conditioned by the

interplay of spin-dependent tunneling, spin accumulation and various spin states that mediate the current, one may expect that in the case of multi-dot structures, where some high-spin molecular states may form, the behavior of the TMR will be modified compared to that observed in the case of single and double dots.

To prove the above statement, in this paper we address the problem of tunneling through chains of quantum dots, consisting of three coherent dots, weakly coupled to external ferromagnetic leads. Very recently the transport properties of triple quantum dots have become a subject of intensive studies due to various interesting effects that emerge in such structures [32–50]. In particular, triple dots enable the investigation of spin-entangled currents [32], dark states [37, 41] or various interference effects [34, 39]. Although nonmagnetic properties of multi-dot structures have already been addressed both theoretically and experimentally, very little is known about their magnetic transport properties [51]. The goal of this paper is therefore to discuss the spin-polarized transport through coherent triple quantum dots. In particular, by employing the real-time diagrammatic technique, we calculate the current, differential conductance, TMR and shot noise in both the sequential and cotunneling regimes. We show that transport characteristics strongly depend on the strength of the interdot correlations, which determines the spatial distribution of electron wavefunctions in the chain. In the case of strong Coulomb correlations, we find that the TMR may take values larger than the Julliere TMR, which is associated with tunneling through high-spin molecular states of the quantum dot system. Moreover, we also predict negative TMR, due to an increased tunneling current in the antiparallel configuration, associated with spin accumulation in the chain. In addition, we show that these effects may be accompanied with super-Poissonian shot noise and negative differential conductance (NDC). On the other hand, in the case of weak interdot Coulomb correlations, the TMR is always positive and not larger than the Julliere TMR, while we still observe super-Poissonian shot noise in the Coulomb blockade regime and negative differential conductance. Although here we consider chains consisting of only three quantum dots, similar behavior may also be observed in longer chains where transport occurs through high-spin molecular states and is governed by various selection rules.

This paper is organized as follows. In the second section we describe the Hamiltonian of the quantum dot chain and briefly discuss the method used in the calculations. Section 3 is devoted to numerical results, where we first analyze the transport characteristics in the case of strong interdot Coulomb correlations and then proceed to discuss the transport behavior in the case of weak interdot correlations. Finally, the conclusions are given in section 4.

2. Theoretical description

2.1. The model

The schematic of a chain consisting of three quantum dots coupled to ferromagnetic leads is shown in figure 1. It is assumed that the magnetizations of the leads are oriented collinearly, so that the system can be either in the parallel or antiparallel magnetic configuration. The Hamiltonian of the system is given by

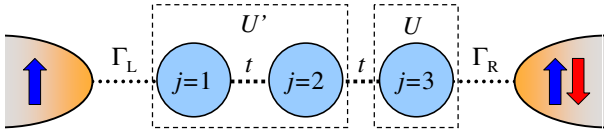

Figure 1. The schematic of a chain consisting of three single-level quantum dots connected to external ferromagnetic leads. The hopping between neighboring dots is denoted by t, U' and U are the interdot and intradot Coulomb correlation energies, while $\Gamma_{\rm L}$ and $\Gamma_{\rm R}$ denote the couplings to the left and right leads. The magnetizations of the leads are assumed to form either parallel or antiparallel magnetic configurations, as sketched in the figure.

$$H = H_{\rm lead} + H_{\rm tun} + H_{\rm chain}, \tag{1}$$

where the first part corresponds to noninteracting itinerant electrons in the left ($r = {\rm L}$) and right ($r = {\rm R}$) lead, $H_{\rm lead} = \sum_r \sum_{\mathbf{k}\sigma} \varepsilon_{r\mathbf{k}\sigma} c^\dagger_{r\mathbf{k}\sigma} c_{r\mathbf{k}\sigma}$, where $\varepsilon_{r\mathbf{k}\sigma}$ is the energy of an electron with the wavevector $\mathbf{k}$ and spin σ in the lead r and $c^\dagger_{r\mathbf{k}\sigma}$ ($c_{r\mathbf{k}\sigma}$) denotes the respective creation (annihilation) operators. The second term of equation (1) accounts for the tunneling processes between the leads and the quantum dot chain:

$$H_{\rm tun} = \sum_{\mathbf{k}\sigma} (t_{\rm L} c^\dagger_{{\rm L}\mathbf{k}\sigma} d_{1\sigma} + t_{\rm R} c^\dagger_{{\rm R}\mathbf{k}\sigma} d_{3\sigma} + {\rm h.c.}), \tag{2}$$

where t_r denotes the tunnel matrix elements between the lead r and the respective dot and $d_{j\sigma}$ destroys a spin-σ electron in the dot j ($j = 1, 2, 3$). Note that the first dot is coupled to the left lead, while the third dot is connected to the right lead, see figure 1. The strength of the coupling of the quantum dot chain to the spin-majority (spin-minority) electron band of the rth lead is given by $\Gamma_r^{+(-)} = 2\pi |t_r|^2 \rho_r^{+(-)} = \Gamma_r(1 \pm p_r)$, where $\Gamma_r = (\Gamma_r^+ + \Gamma_r^-)/2$, while $\rho_r^{+(-)}$ and p_r are the spin-dependent density of states for majority (minority) spin band and spin polarization in the lead r, respectively. In the following we assume $\Gamma_{\rm L} = \Gamma_{\rm R} \equiv \Gamma/2$ and $p_{\rm L} = p_{\rm R} \equiv p$.

Finally, the last term of the Hamiltonian describes the chain consisting of three quantum dots which is given by

$$\begin{aligned} H_{\rm chain} = & \sum_j \sum_\sigma \varepsilon_j n_{j\sigma} + \sum_j U_j n_{j\uparrow} n_{j\downarrow} \\ & + U' \sum_{\sigma\sigma'} (n_{1\sigma} n_{2\sigma'} + n_{2\sigma} n_{3\sigma'}) \\ & + t \sum_\sigma (d^\dagger_{1\sigma} d_{2\sigma} + d^\dagger_{2\sigma} d_{3\sigma} + {\rm h.c.}), \end{aligned} \tag{3}$$

with $n_{j\sigma} = d^\dagger_{j\sigma} d_{j\sigma}$ being the particle number operator on dot j, while ε_j and U_j denote the single-particle energy and on-level Coulomb correlation in dot j, respectively. The third part of $H_{\rm chain}$ corresponds to the interdot Coulomb interaction, whose strength is given by U', while t describes the interdot hopping. As we are interested in a rather low bias voltage regime, it is justifiable to assume that the dot energy levels are independent of the bias voltage. This assumption has also been verified numerically and even if one assumes a voltage drop on

the outer dots of the order of 10%, the current flowing through the system becomes only very slightly modified as compared to that in the case of zero voltage drop. Therefore, for the sake of clarity in further discussion, we take the energy-independent dot levels. Furthermore, we also assume that the system is symmetric, i.e. $\varepsilon_j \equiv \varepsilon$ and $U_j \equiv U$ ($j = 1, 2, 3$).

2.2. The method

In order to calculate the spin-polarized transport through a chain of three coherent quantum dots in the sequential and cotunneling regimes, we employ the real-time diagrammatic technique [7, 52, 53]. It generally consists in a perturbative expansion of the density matrix of the system and the operators of interest (for example, the current operator) with respect to the coupling strength Γ. Time evolution of the reduced density matrix is given by a sequence of irreducible self-energy blocks, $\Sigma_{\chi\chi'}$, on the Keldysh contour, corresponding to various transition events between the many-body states $|\chi\rangle$ and $|\chi'\rangle$ of the quantum dot chain. On the other hand, the full propagation of the reduced density matrix is given by the Dyson equation, which can be further transformed into a general kinetic equation. In a steady state the kinetic equation is simply given by $(\tilde{\mathbf{\Sigma}}\mathbf{P})_\chi = \Gamma\delta_{\chi\chi_0}$ and enables the calculation of occupation probabilities P_χ for the system to be in a many-body state $|\chi\rangle$. Here, $\mathbf{P}$ is the probability vector, while the matrix $\tilde{\mathbf{\Sigma}}$ is given by the self-energy matrix $\mathbf{\Sigma}$ with one arbitrary row χ_0 replaced by $(\Gamma, \ldots, \Gamma)$ due to normalization, $\sum_\chi P_\chi = 1$. The current flowing through the system can be then found from [52]

$$I = -\frac{ie}{2\hbar}\mathrm{Tr}\{\mathbf{\Sigma}^{\mathrm{I}}\mathbf{P}\}, \tag{4}$$

where $\mathbf{\Sigma}^{\mathrm{I}}$ denotes the modified self-energy matrix $\mathbf{\Sigma}$ so as to take into account the number of electrons transferred through the system.

To calculate the transport properties order by order in tunneling processes, we expand the self-energy matrices, $\mathbf{\Sigma} = \mathbf{\Sigma}^{(1)} + \mathbf{\Sigma}^{(2)} + \cdots$, $\mathbf{\Sigma}^{\mathrm{I}} = \mathbf{\Sigma}^{\mathrm{I}(1)} + \mathbf{\Sigma}^{\mathrm{I}(2)} + \cdots$, and the occupations, $\mathbf{P} = \mathbf{P}^{(0)} + \mathbf{P}^{(1)} + \cdots$, respectively. The self-energies in respective order can then be calculated using the corresponding diagrammatic rules [7, 52]. The first order of expansion corresponds to the sequential tunneling, whereas the second one to cotunneling. In this analysis we have calculated the self-energies up to the second order of the perturbation series, so that we are able to resolve the transport properties both in the sequential and cotunneling regimes [15]. The sequential tunneling dominates transport above a threshold voltage and is exponentially suppressed in the Coulomb blockade regime [54]. In the blockade regime, on the other hand, the dominant contribution to the current comes from cotunneling processes [55], which take place through virtual states of the system and are only algebraically suppressed in the Coulomb blockade. As the influence of cotunneling on transport for bias voltages above the threshold for sequential tunneling is rather minor, the inclusion of second-order processes is crucial for a proper description of transport in the blockade regimes.

In addition, in the following we will also analyze the zero-frequency current noise [56], $S = \int_{-\infty}^{\infty} \mathrm{d}t(\langle\hat{I}(t)\hat{I}(0) + \hat{I}(0)\hat{I}(t)\rangle - 2\langle\hat{I}\rangle^2)$, where $\hat{I}$ is the current operator, $\hat{I} = (\hat{I}_{\mathrm{R}} - \hat{I}_{\mathrm{L}})/2$, with $\hat{I}_{\mathrm{L(R)}} = -\mathrm{i}(e/\hbar)t_{\mathrm{L(R)}}\sum_{\mathbf{k}\sigma}(c^\dagger_{\mathrm{L(R)}\mathbf{k}\sigma}d_{1(3)\sigma} - d^\dagger_{1(3)\sigma}c_{\mathrm{L(R)}\mathbf{k}\sigma})$ being the current flowing from the first (third) dot to the left (right) lead. The formula for current noise derived within the real-time diagrammatic technique can be found in [53].

3. Numerical results

In the following we will discuss the numerical results on the current, differential conductance, tunnel magnetoresistance and the shot noise of a chain of three coherent single-level quantum dots in both the linear and nonlinear response regimes. Transport characteristics of such systems strongly depend on the internal parameters, in particular, on the ratio between interdot Coulomb repulsion U' and the hopping between the dots t, provided that $U > U'$, $|t|$. The ratio can be tuned experimentally, for example, by changing the height of the barrier between the dots [57]. When the interdot Coulomb correlations are relatively strong, $U'/|t| > 1$, the electrons in the ground state of the chain will be mostly occupying the outermost dots. On the other hand, for weak interdot Coulomb interactions, $U'/|t| < 1$, this tendency will not be observed. Thus, depending on $U'/|t|$, the spatial distribution of the many-body chain states may become strongly modified. In this paper we will therefore discuss the transport characteristics in the two above-mentioned situations. Furthermore, we also note that, due to many intrinsic parameters of the system, there are a variety of transport regimes where different transport behavior can be observed. In the following, we will thus present general density plots: however, only the most interesting transport features will be discussed in greater detail.

3.1. The case of strong interdot Coulomb interactions

Figure 2 shows various transport characteristics of a quantum dot chain as a function of bias voltage V and the position of the dots' levels ε. Because the position of the levels can be experimentally changed by sweeping the gate voltage, figure 2 effectively presents a bias and gate voltage dependence of transport characteristics. The total (first plus second order) differential conductance for the parallel (G_{P}) and antiparallel (G_{AP}) magnetic configurations is shown in figures 2(a) and (b), respectively. First of all, one can see that the differential conductance displays a characteristic Coulomb diamond pattern, with Coulomb blockade regimes at low transport voltages. By lowering the position of the dots' levels the chain becomes consecutively occupied with electrons. In the case considered here, the quantum dot chain can accommodate up to six electrons, i.e. each dot can be doubly occupied. For such values of ε when the two neighboring charge states become degenerate, there is a peak in the linear conductance. On the other hand, with increasing the bias voltage, out of the Coulomb blockade regime, there are additional lines visible in the differential conductance associated with tunneling through excited states of the system. Furthermore, due to the contact

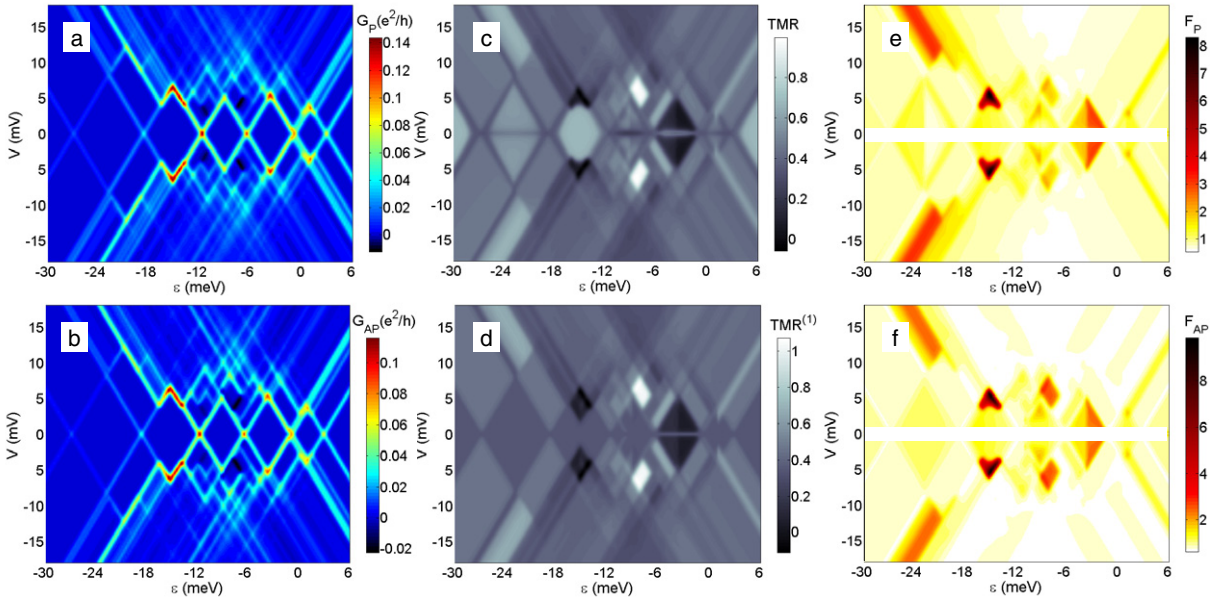

Figure 2. The total (first plus second order) differential conductance in the parallel (a) and antiparallel (b) alignment, the total TMR (c), the TMR calculated using only first-order processes (d) and the total Fano factor for parallel (e) and antiparallel (f) configurations of the system. The figures were calculated for the case where the interdot Coulomb interaction is larger than the interdot hopping, $U'/|t| > 1$. The parameters are: $U' = 4$ meV, $t = -2$ meV, $U = 10$ meV, $k_BT = 0.15$ meV, $\Gamma = 0.1$ meV and $p = 0.5$. The Fano factor at low bias voltages diverges. Therefore this transport regime is marked with a white stripe in (e) and (f).

with ferromagnetic leads, the tunneling processes in the system become spin-dependent and, consequently, transport depends on the magnetic configuration of the system. In the parallel configuration the majority (minority) electrons of one lead tunnel to the majority (minority) spin band of the other lead, whereas in the antiparallel configuration they tunnel to the minority (majority) spin band. This is why the conductance in the antiparallel configuration is generally suppressed as compared to that in the parallel configuration, $G_P > G_{AP}$, see figures 2(a) and (b). This difference in turn gives rise to nonzero tunnel magnetoresistance which is plotted in figure 2(c).

The TMR reflects the change of systems' transport properties when switching the magnetic configuration of the device from a parallel to an antiparallel one. It is qualitatively defined as [1, 2, 4] TMR $= I_P/I_{AP} - 1$, where I_P (I_{AP}) is the current flowing through the system in the parallel (antiparallel) magnetic configuration. Usually the conductance in the parallel configuration is larger than that in the antiparallel one, giving rise to positive TMR. In particular, for a single ferromagnetic tunnel junction the TMR can be described by the Julliere model [1], $\mathrm{TMR}^{\mathrm{Jull}} = 2p^2/(1-p^2)$ ($\mathrm{TMR}^{\mathrm{Jull}} = 2/3$ for $p = 0.5$ assumed in calculations). Intuitively, one may expect that placing a quantum dot molecule between the two leads (where tunneling processes are generally incoherent) will decrease the TMR. This is, in fact, what is observed in most quantum dot structures—for symmetric systems and in the absence of magnetic field, the TMR in the weak coupling regime is positive and not larger than $\mathrm{TMR}^{\mathrm{Jull}}$ [7, 16]. In the case of tunneling through quantum dot chains considered here, however, we predict a nontrivial behavior of the TMR. Depending on the transport regime, we find both the TMR enhanced above the Julliere value as well as the negative TMR effect, see figure 2(c). The mechanisms responsible for these effects will be discussed in more detail in the following.

We also note that the TMR is directly related to the ratio between the currents in the two magnetic configurations, so that its magnitude does not necessarily depend on the magnitude of the tunneling current. This makes the TMR a very sensitive quantity for analyzing the transport properties in various regimes, especially where sequential tunneling is suppressed due to Coulomb correlations and transport occurs mainly through higher-order tunneling processes. For comparison, in figure 2(d) we have also plotted the TMR calculated using only the first-order tunneling processes, $\mathrm{TMR}^{(1)}$. It can be seen that cotunneling processes modify the TMR mainly in the blockade regimes and give rise to strong dependence of the TMR on the occupation number of the quantum dot chain. On the other hand, out of the blockade regimes, the current is predominantly mediated by sequential tunneling and one finds that TMR and $\mathrm{TMR}^{(1)}$ become comparable, although not equal.

In addition, we have also calculated the Fano factor, $F = S/S_p$, in both magnetic configurations, see figures 2(e) and (f). The Fano factor describes the deviation of the shot noise from its Poissonian value, $S_p = 2e|I|$, which is characteristic of uncorrelated tunneling. When transport is mediated only by elastic cotunneling processes, the noise is Poissonian, $F \to 1$. However, once the spin–flip cotunneling is allowed the noise can be enhanced to become super-Poissonian, $F > 1$, due to bunching of inelastic processes [58]. Furthermore, in the sequential tunneling regime, transport is mainly dominated by Coulomb correlations which decrease the noise and the Fano factor is generally sub-Poissonian, $F < 1$ [59]. This

Table 1. The charge Q and the total spin S of three quantum dots coupled in the series, the dimension of the respective $\{Q, S\}$ blocks, D, degeneracy of states, d, and ground state energies, $E^{\rm G}_{Q,S}$. The analytical formulae for ground state energies of larger blocks are rather lengthy; therefore here we only state which states have lower energy for a given Q. The explicit matrices for Hamiltonian blocks are given in the appendix.

n	Q	S	D	d	Ground state energies
1	0	0	1	1	$E^{\rm G}_{0,0} = 0$
2	1	$\frac{1}{2}$	3	2	$E^{\rm G}_{1,\frac{1}{2}} = \varepsilon - \sqrt{2}\lvert t\rvert$
3	2	0	6	1	$E^{\rm G}_{2,0} \lesssim E^{\rm G}_{2,1}$
4	2	1	3	3	$E^{\rm G}_{2,1} = 2\varepsilon + \frac{1}{2}U' - \sqrt{2t^2 + (U'/2)^2}$
5	3	$\frac{1}{2}$	8	2	$E^{\rm G}_{3,\frac{1}{2}} \lesssim E^{\rm G}_{3,\frac{3}{2}}$
6	3	$\frac{3}{2}$	1	4	$E^{\rm G}_{3,\frac{3}{2}} = 3\varepsilon + 2U'$
7	4	0	6	1	$E^{\rm G}_{4,0} \lesssim E^{\rm G}_{4,1}$
8	4	1	3	3	$E^{\rm G}_{4,1} = 4\varepsilon + U + \frac{7}{2}U' - \sqrt{2t^2 + (U'/2)^2}$
9	5	$\frac{1}{2}$	3	2	$E^{\rm G}_{5,\frac{1}{2}} = 5\varepsilon + 2U + 5U' - \sqrt{2t^2 + U'^2}$
10	6	0	1	1	$E^{\rm G}_{6,0} = 6\varepsilon + 3U + 8U'$

behavior can be, in fact, observed in figures 2(e) and (f), where in the cotunneling regime the Fano factor can take large super-Poissonian values, while in the sequential tunneling regime it becomes rather suppressed. It can also be seen that the general behavior of the Fano factor in the parallel ($F_{\rm P}$) and antiparallel ($F_{\rm AP}$) magnetic configurations is quite similar, although the magnitude of the noise is larger in the antiparallel configuration. On the other hand, in the low bias voltage regime, the noise is dominated by thermal noise while the current tends to zero, which leads to a divergency in the Fano factor. Therefore this transport regime is marked with white stripes in figures 2(e) and (f).

3.1.1. Linear response regime. In the linear response regime, the transport behavior is mainly conditioned by the ground state of the system and its evolution when changing the position of the dot levels. The ground state energies $E^{\rm G}_{Q,S}$ together with respective quantum numbers of states $\{Q, S\}$ are shown in table 1, with

$$Q = \sum_{j\sigma} n_{j\sigma}, \qquad \vec{S} = \tfrac{1}{2}\sum_{j\sigma\sigma'} d^\dagger_{j\sigma}\vec{\sigma}_{\sigma\sigma'}d_{j\sigma'}, \tag{5}$$

denoting the total charge and total spin of the quantum dot chain. Because in the absence of external magnetic field the Hamiltonian of the chain, equation (3), commutes with Q and S^2, one can solve the eigenvalue problem by diagonalizing $H_{\rm chain}$ in respective blocks $\{Q, S\}$. Furthermore, by using the full spin $SU(2)$ symmetry the size of the Hilbert space is effectively reduced from 64 to 35 multiplets, which may be crucial for an analytical discussion of decoupled quantum dot chains. In numerical calculations, however, we have used the 64-state space with the following many-body states: $|\chi\rangle = |\chi_1\chi_2\chi_3\rangle$, where $\chi_j = 0, \uparrow, \downarrow, {\rm d}$ denotes the state with zero electrons, one spin-up, spin-down electron and two electrons on the dot j. This is because in the case of the spin-dependent coupling to ferromagnetic leads, the Hamiltonian

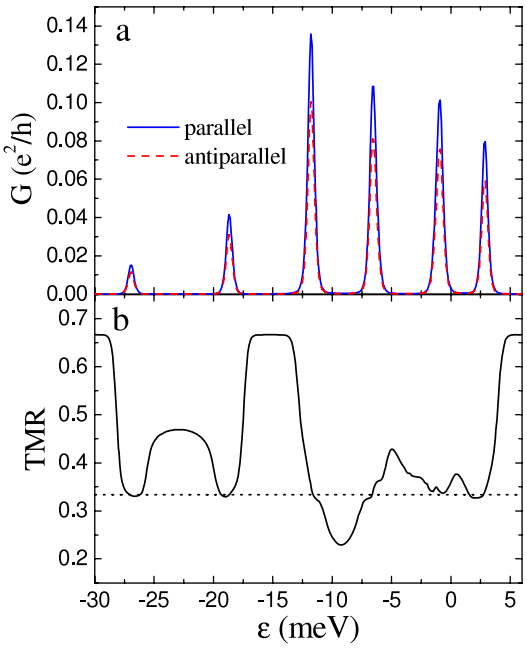

Figure 3. The linear conductance (a) in the parallel (solid line) and antiparallel (dashed line) magnetic configurations and linear response TMR (b) as a function of the dots' level position ε. The parameters are the same as in figure 2. The dotted line in (b) shows the linear TMR calculated by using only first-order processes—sequential TMR is constant and given by ${\rm TMR}^{(1)} = p^2/(1-p^2)$.

of the whole system possesses only the S_z symmetry. In table 1 we show the corresponding quantum numbers, the dimension of the Hamiltonian blocks, the degeneracy of states and the ground state energies of the decoupled quantum dot chain. It turns out that the ground state energies $E^{\rm G}_{Q,S}$ for smaller blocks can be easily calculated. However, for larger blocks the formulae become too lengthy to be presented here. We thus list the explicit expressions for low-dimension Hamiltonian blocks, while for the other blocks we just state which energy is the lowest one in the respective charge sector Q. The explicit matrices for Hamiltonian blocks $H_{Q,S}$ together with the definition of states for total charge and total spin symmetries can be found in the appendix.

The linear conductance as well as the total TMR are shown in figures 3(a) and (b). The linear conductance displays characteristic resonance peaks whenever two neighboring charge states become degenerate. The resonance energies can be estimated from table 1 by solving $\min\{E^{\rm G}_{Q+1,S}\} - \min\{E^{\rm G}_{Q,S}\} = 0$, where one needs to take the minimum energy for given Q. The conductance in the parallel configuration is larger than the conductance in the antiparallel configuration, see figure 3(a), which results in a positive linear TMR, see figure 3(b). For comparison we have also plotted the TMR obtained using only first-order tunneling processes, which is constant and given by ${\rm TMR}^{(1)} = p^2/(1-p^2)$, see the dotted line in figure 3(b). The total TMR, on the other hand, shows a nontrivial dependence on the position of the dots' levels ε. As shown in the case of single quantum dots [7, 16], the magnitude of linear TMR is directly related to the type of cotunneling processes that drive the current in the respective

transport regimes. Among various cotunneling events, one can distinguish processes that affect the magnetic state of the quantum dot system (inelastic spin–flip processes) and the ones that do not affect the quantum dot chain (elastic non-spin-flip processes). In the case when each dot of the chain is either empty or doubly occupied, only elastic processes are possible. However, in the other cases, the spin-flip processes also become allowed.

When the chain is empty ($Q = 0$) or fully occupied ($Q = 6$), the TMR is maximal and equal to the Julliere value, TMR $= 2p^2/(1-p^2)$, see figure 3(b). This is related to the fact that in these transport regimes only the non-spin-flip cotunneling processes are allowed and transport is fully coherent—the cotunneling electrons are not scattered at the chain at all. Interestingly, also for $Q = 4$ the TMR becomes equal to $\mathrm{TMR}^{\mathrm{Jull}}$, which indicates that only elastic cotunneling contributes to the linear conductance. In fact, for $Q = 4$ the ground state of the chain is $S = 0$, see table 1. Furthermore, for assumed parameters, i.e. in the case of strong interdot correlations, $U'/t > 1$, it turns out that in the ground state the chain is occupied with two electrons in the outermost dots, so that the ground state is $|\mathrm{d0d}\rangle$. In this case only the non-spin-flip cotunneling is allowed, which yields the maximum TMR. However, the situation changes once the spin-flip processes become possible, which happens in the other transport regimes. In particular, for $Q = 1, 2, 3$, the linear TMR becomes suppressed to approximately half of $\mathrm{TMR}^{\mathrm{Jull}}$ and its dependence on ε is rather complex. In these regimes the current is mainly mediated by inelastic spin-flip cotunneling. For $Q = 5$, on the other hand, the TMR becomes slightly enhanced, although it is still lower than $\mathrm{TMR}^{\mathrm{Jull}}$. Because for $Q = 5$ the ground state is a doublet $|\mathrm{d}\sigma\mathrm{d}\rangle$, transport is due to both elastic and inelastic processes—the former (latter) ones tend to increase (decrease) the TMR, so that the magnitude of the TMR is between the values corresponding to the $Q = 1, 2, 3$ and $Q = 0, 4, 6$ transport regimes. Finally, we also note that at resonances the total TMR decreases to the value approximately given by $\mathrm{TMR}^{(1)}$, while as for resonant energies the first-order processes become possible and are dominant.

3.1.2. Enhanced TMR and negative differential conductance. The bias dependence of the current, differential conductance, Fano factor and TMR is shown in figure 4. The transport characteristics were calculated for $\varepsilon = -7.5$ meV, see also figure 2, which corresponds to the case when at equilibrium the quantum dot chain is in the spin doublet state, $\{Q = 3, S = \frac{1}{2}\}$, so that the ground state is doubly degenerate. With increasing bias voltage, more and more states start participating in transport and the current increases. However, it can be seen that the bias dependence of the current is not monotonic—after the first Coulomb step, the current starts to decrease with V, leading to negative differential conductance (NDC), which is present in both magnetic configurations, see figure 4(b). The suppression of the current is associated with selection rules that govern the respective sequential transitions, i.e. only the transitions that change the total charge of the chain by 1 and the total spin by $\frac{1}{2}$ are allowed. When raising the transport voltage, the following excited states $\{Q, S\}$ become

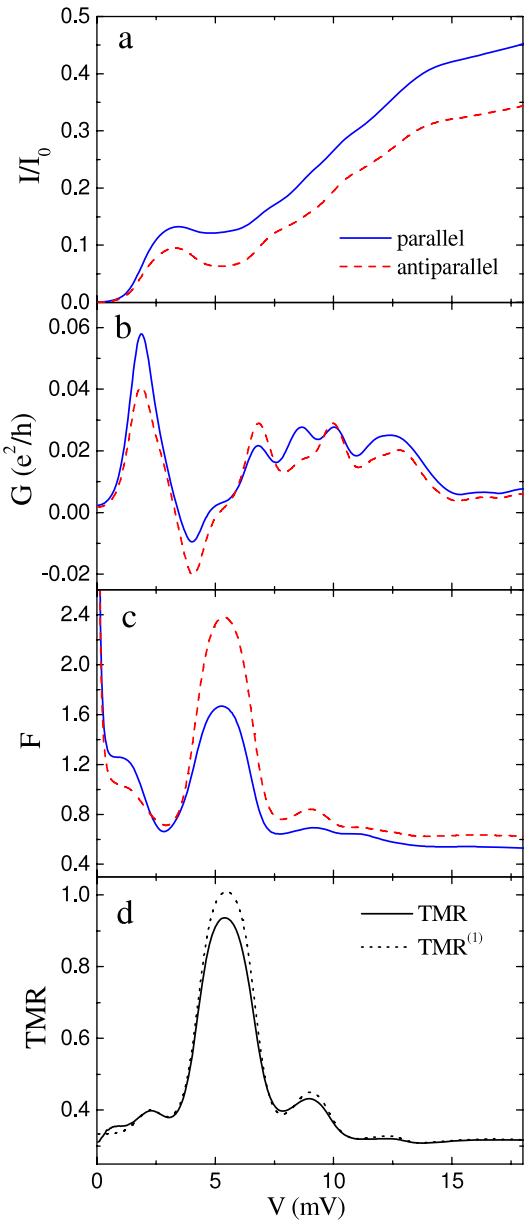

Figure 4. The bias voltage dependence of the current (a), differential conductance (b), Fano factor (c) in the parallel (solid line) and antiparallel (dashed line) magnetic configurations and the resulting TMR (d) for $\varepsilon = -7.5$ meV. The other parameters are the same as in figure 2 and I_0 denotes the maximum current given by $I_0 = e\Gamma/\hbar$.

active in transport: $\{2, 0\}$ singlet and $\{2, 1\}$ triplet, then $\{3, \frac{1}{2}\}$ doublet, and then $\{3, \frac{3}{2}\}$ quadruplet, respectively. Although the sequential transitions between $Q = 3$ doublet and $Q = 2$ singlet and triplet are possible, the transitions between $Q = 3$ doublet and $Q = 3$ quadruplet are prohibited as they obey neither the charge nor the spin selection rules. In fact, once the system gets trapped in the quadruplet state, transport becomes suppressed, see figure 4(a) for $V \approx 5$ mV, which leads to negative differential conductance. This is because transitions involving the $\{3, \frac{3}{2}\}$ state can occur only through tunneling from/to the triplet state $\{2, 1\}$. In the case of $U/|t'| > 1$, the two electrons in the triplet state are localized in the outermost

dots, while in the quadruplet state the three electrons are distributed uniformly between the dots. Thus, for a transition between $\{3, \frac{3}{2}\}$ and $\{2, 1\}$ to occur, one needs to put or remove an electron from the middle dot, which is however suppressed as $(t/U')^2$. On the other hand, tunneling processes in which the state of the system changes between the $Q = 3$ doublet and $Q = 2$ singlet are rather independent of the ratio t/U', as they can occur through the outermost dots. Consequently, transitions involving the quadruplet state are relatively slow, while the other ones are much faster. The competition between such *slow* and *fast* transport channels may in turn lead to large current fluctuations [35]. This can be seen in figure 4(c), where for voltages corresponding to the transport regime where the current is suppressed, super-Poissonian shot noise is observed. When increasing the bias voltage further, more excited states become available for transport and the current starts increasing again, see figure 4(a), while the shot noise becomes suppressed to the sub-Poissonian value, which is typical of charge-correlated sequential transport, see figure 4(c).

In the antiparallel configuration, on the other hand, due to the asymmetry of tunneling processes between the left and right leads, there is a nonequilibrium spin accumulation in the chain. For positive bias voltages, the occupation probability of highest-weight spin states is much increased compared to the other components of a particular state. This is because the spin-up electrons tunneling from the left lead to the chain and the spin-down electrons tunneling out of the chain to the right lead belong to the majority-spin bands, and the positive spin component becomes accumulated in the chain. Consequently, fewer states are available for transport compared to the parallel configuration, so that in the antiparallel configuration the transport channel involving the quadruplet state $\{3, \frac{3}{2}\}$ becomes even less transmitting. This leads to several interesting features. First of all, the current is more suppressed in the antiparallel configuration than in the parallel one, which leads to an enhanced NDC, see figure 4(b). On the other hand, this more effective current suppression also reflects itself in an enhanced super-Poissonian shot noise, see figure 4(c). Furthermore, for voltages where the current is suppressed we observe the TMR enhanced above the Julliere value. The TMR in this transport regime is approximately given by $\mathrm{TMR} \approx \frac{3}{2}\mathrm{TMR}^{\mathrm{Jull}}$, see figure 4(d). As shown in previous considerations, such an enhancement of TMR in serial quantum dots weakly coupled to external leads can occur mainly in asymmetric systems or in the presence of an external magnetic field [15, 16]. Here, we observe $\mathrm{TMR} > \mathrm{TMR}^{\mathrm{Jull}}$ in the absence of a magnetic field and for a fully symmetric system. This is just a generic feature of transport through chains of quantum dots, where due to selection rules the system may be trapped in some high-spin states.

3.1.3. Negative TMR and super-Poissonian shot noise. Another interesting transport behavior can be observed in the case where the chain is in the ground state with four electrons. The current, differential conductance, shot noise and TMR as a function of the bias voltage for $\varepsilon = -15$ meV are shown in figure 5. Due to large interdot Coulomb correlations, $U'/|t| > 1$, the ground state is non-degenerate,

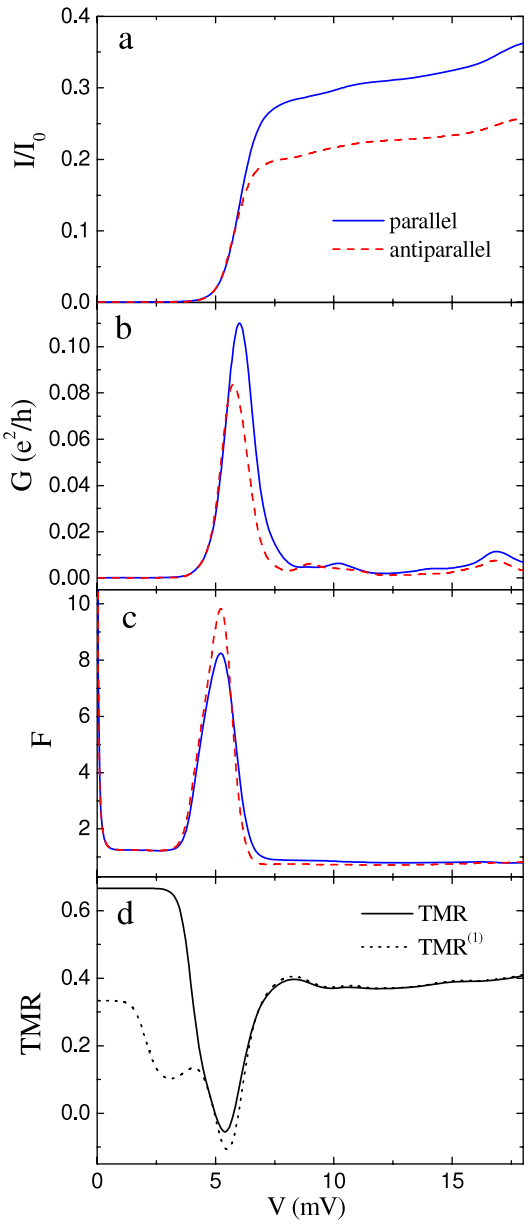

Figure 5. The bias voltage dependence of the current (a), differential conductance (b), Fano factor (c) in the parallel (solid line) and antiparallel (dashed line) magnetic configurations and the resulting TMR (d) for $\varepsilon = -15$ meV and the parameters as in figure 2.

with doubly occupied outermost dots, $|\mathrm{d0d}\rangle$. The nearest excited states are, respectively, doublets $\{3, \frac{1}{2}\}$ and $\{5, \frac{1}{2}\}$, and triplet $\{4, 1\}$. These states are relatively close to each other and start taking part in transport for voltages around the threshold for sequential tunneling. At low bias voltages the system is in the Coulomb blockade, see figures 5(a) and (b), and transport is due to elastic cotunneling processes, which yield the Poissonian shot noise and TMR given by the Julliere value, see figures 5(c) and (d). The situation changes once the transport voltage approaches the threshold, $V \approx 5$ mV; then the TMR suddenly drops and changes sign, while the shot noise becomes strongly enhanced. This is associated with tunneling processes that become allowed in this transport regime. First of all, the inelastic cotunneling processes become possible

for each doublet state, i.e. $\{3, \frac{1}{2}\}$ and $\{5, \frac{1}{2}\}$. Furthermore, around the threshold voltage, the sequential processes also start participating in transport. The first-order transitions occur first between the $Q = 4$ singlet and $Q = 3$, $Q = 5$ doublets. It is worth noting that the spatial distribution of the wavefunction is different for these two doublets. For $Q = 3$ the electrons are equally distributed between the three dots, while for $Q = 5$ the outermost dots are fully occupied while the middle dot is singly occupied to minimize the interdot correlations. Consequently, the transport channel involving the state $\{5, \frac{1}{2}\}$ is slower than that involving the state $\{3, \frac{1}{2}\}$, similarly as in the case discussed in the previous subsection. It turns out that the interplay of various first- and second-order tunneling processes, where particular events occur at different rates, which exist for transport voltages around the threshold for sequential tunneling, leads to large current fluctuations. As a result, we observe an enhanced super-Poissonian shot noise in both magnetic configurations of the system, see figure 5(c). On the other hand, when the voltage increases further, sequential processes dominate transport and the noise becomes generally sub-Poissonian.

An interesting transport feature visible around the threshold voltage is the negative TMR effect, see figure 5(d). To understand this behavior, one needs to realize a very delicate difference between probability distributions in the two magnetic configurations. In the Coulomb blockade regime the chain is in the singlet state $|\mathrm{d0d}\rangle$ with probability equal to unity, irrespective of magnetic configuration of the system. However, once the bias voltage approaches the threshold voltage, the occupation probability of states $\{3, \frac{1}{2}\}$, $\{5, \frac{1}{2}\}$ and $\{4, 1\}$ starts slowly increasing. In addition, it turns out that in the antiparallel configuration the probability of the highest-weight quadruplet state is also nonzero, and it is slightly larger than the occupation probabilities of the above-mentioned doublets and triplet. The enhanced occupation probability of $\{3, \frac{3}{2}\}$ is purely due to nonequilibrium spin accumulation. It is thus not present in the parallel configuration. This is, in fact, what is crucial for the occurrence of negative TMR. In the antiparallel configuration the current can, in addition, flow due to cotunneling and thermally activated first-order transitions involving the quadruplet state, which is not possible in the parallel configuration. As a result, the current in the antiparallel configuration becomes larger than the current in the parallel configuration, yielding a negative TMR effect. This can also be seen in the differential conductance where the first peak in the antiparallel configuration occurs at slightly lower bias voltage than in the parallel one, see figure 5(b). With increasing the bias voltage further, the excited states start participating in transport and the system apparently exhibits a *normal* spin-valve behavior [6, 7], with the current in the parallel configuration larger than in the antiparallel one and, thus, with positive TMR, see figure 5(d). It is interesting to note that the increased occupation probability of the highest-spin component of the quadruplet state in the antiparallel configuration was also responsible for the enhanced TMR effect discussed in the previous subsection, whereas here it lead to negative TMR. The negative TMR, however, occurs on the edge of the Coulomb blockade regime, while the enhanced TMR develops in the sequential tunneling regime.

3.2. The case of weak interdot Coulomb interaction

The differential conductance, TMR and Fano factor in the case of $U'/|t| < 1$ are shown in figure 6. For $U'/|t| < 1$, the electrons in particular states are distributed rather uniformly over the three dots, contrary to the previous case where electrons were localized in the outermost dots to minimize the Coulomb correlation energy. This results in a more symmetric behavior of transport characteristics with respect to the middle of the Coulomb blockade regime with $Q = 3$, which is due to particle–hole symmetry. Moreover, as most of the effects observed for $U'/|t| > 1$ were mainly associated with spatial distribution of the wavefunction, one may expect their strong dependence on the ratio $U'/|t|$. This is, in fact, what can be observed. For example, when $U'/|t| < 1$, the negative TMR and TMR enhanced above the Julliere value are not present, although super-Poissonian shot noise and negative differential conductance can still be found in some transport regimes. Of course, the difference between transport characteristics in the case of weak and strong interdot correlations reveals itself mainly in transport regimes where the states with more than a single electron become relevant, see figures 2 and 6.

The differential conductance in the parallel and antiparallel configurations is shown in figures 6(a) and (b), respectively. First of all, we note that, because the energy of interdot correlations is now changed, the Coulomb diamond structure is different from that shown in figure 2. The largest Coulomb diamond develops for $Q = 3$, while the size of other diamonds is much decreased, except for empty and fully occupied chains, see figures 6(a) and (b). The conductance in the parallel configuration is larger than in the antiparallel one and the TMR is positive in the whole range of bias voltage V and level position ε, see figure 6(c). For comparison, the TMR calculated using only the sequential tunneling processes is shown in figure 6(d). The main difference between the density plots for the total TMR and $\mathrm{TMR}^{(1)}$ can be seen in the Coulomb blockade regimes where cotunneling dominates the current. It can be seen that the total TMR in the linear response regime displays nontrivial dependence on the occupation number of the chain. For empty and fully occupied chains, the TMR is given by the Julliere value and it is much suppressed in other blockade regimes due to spin–flip cotunneling processes.

In the nonlinear response regime when at equilibrium the chain was in the charge state $Q = 3$, it is reminiscent of effects found in the case of $U'/|t| > 1$, see figure 4. Now, one can also observe an enhanced TMR, although its magnitude is slightly lower than the Julliere TMR. This enhanced TMR is accompanied by negative differential conductance and super-Poissonian shot noise, which are more visible in the antiparallel configuration. The mechanism leading to these effects is similar to that discussed in the previous subsection and is mainly associated with a transport channel involving the quadruplet state and spin accumulation in the antiparallel configuration.

Furthermore, in the nonlinear response regime of the Coulomb blockade regime with $Q = 2$, the TMR becomes suppressed, being very close to zero. In this transport regime the chain at equilibrium is in the singlet state $\{2, 0\}$ and the excited states are consecutively $\{2, 1\}$ and $\{1, \frac{1}{2}\}$. On

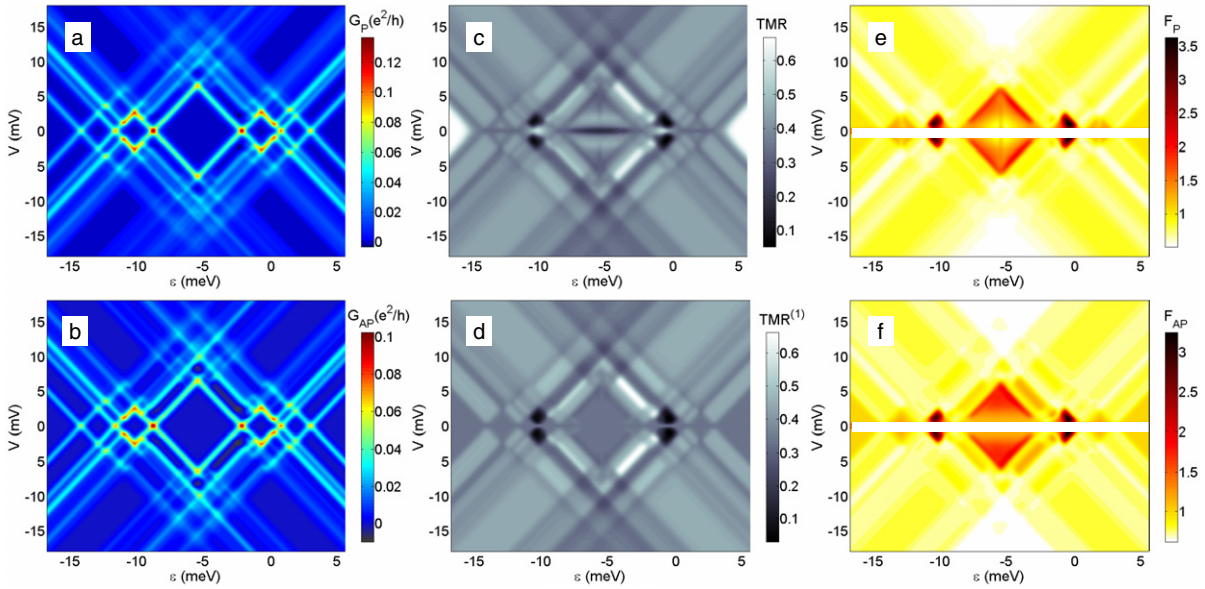

Figure 6. The total differential conductance in the parallel (a) and antiparallel (b) alignment, the total TMR (c), the TMR calculated using only first-order processes (d) and the total Fano factor for parallel (e) and antiparallel (f) configuration of the system for the case when the interdot Coulomb interaction is smaller than the interdot hopping, $U'/|t| < 1$. The parameters are: $U' = 0.5$ meV, $t = -2$ meV, $U = 10$ meV, $k_B T = 0.15$ meV, $\Gamma = 0.1$ meV and $p = 0.5$. The Fano factor at low bias voltage diverges, therefore this transport regime is marked with a white stripe in (e) and (f).

increasing the bias voltage, the occupation probability of excited states starts increasing. It turns out that in the parallel configuration all the components of the $Q = 1$ doublet and $Q = 2$ triplet are relevant, while in the antiparallel configuration, due to spin accumulation, only the highest-weight components are relevant, however with slightly larger occupation probabilities. This leads to an increased current in the antiparallel configuration, so that the currents in the two configurations become roughly comparable, yielding very small TMR. In addition, on raising the bias voltage the shot noise becomes enhanced and reaches a maximum for voltages around the threshold for sequential tunneling, which is associated with bunching of inelastic cotunneling processes. Similar behavior can also be observed for the Coulomb blockade regime with four electrons in the chain, which is due to particle–hole symmetry. It is also interesting to note that the behavior of transport characteristics in the cotunneling regime with $Q = 2$ is very weakly affected by the ratio $U'/|t|$, see figures 2 and 6. However, for Coulomb blockade regimes with more electrons in the ground state, transport properties become completely modified due to different spatial distribution of wavefunctions: compare, for example, the Coulomb blockade regime with $Q = 4$ in figures 2 and 6.

Finally, we also note that in the case of weak interdot correlations the shot noise is rather sub-Poissonian in the whole sequential tunneling regime, irrespective of the magnetic configuration of the system. On the other hand, the super-Poissonian shot noise is only found in the Coulomb blockade regimes where the chain is the charge state with two, three or four electrons, which is due to bunching of inelastic cotunneling processes.

4. Conclusions

We have analyzed the linear and nonlinear transport properties in chains of quantum dots consisting of three coherent single-level quantum dots weakly coupled to external ferromagnetic leads. By employing the real-time diagrammatic technique, we have calculated the current, differential conductance, shot noise and tunnel magnetoresistance in the case of strong ($U'/|t| > 1$) and weak ($U'/|t| < 1$) interdot correlations. By changing the ratio $U'/|t|$, one can effectively change the spatial distribution of electron wavefunctions of the chain. When $U'/|t| > 1$, the electrons tend to be localized in the outermost dots, while for $U'/|t| < 1$ the electrons are distributed rather uniformly over the dots.

In particular, in the case of large interdot correlations we have shown that the TMR strongly depends on the transport regime and can take negative values as well as values exceeding the TMR given by the Julliere model. The enhanced TMR occurs in the nonlinear response regime when the chain is occupied by three electrons at equilibrium and is associated with a suppressed current in the antiparallel configuration due to trapping of the quantum dot chain in some high-spin states. In addition, the suppression of the current gives rise to negative differential conductance and super-Poissonian shot noise. We have also shown that the TMR may change sign and become negative. This happens in the cotunneling regime with four electrons in the chain when the bias voltage approaches the threshold voltage for sequential tunneling. The negative TMR is then associated with increased tunneling through the highest-weight spin state (quadruplet) of the chain. Furthermore, we have also shown that negative TMR is accompanied with large super-Poissonian shot noise due to the interplay between various inelastic cotunneling and sequential processes that start

contributing to the current around the threshold voltage. On the other hand, when the interdot correlations are weak, most of the effects found in the case of $U'/|t| > 1$ become smeared out. In particular, the negative TMR and TMR enhanced above the Julliere value are not present, although super-Poissonian shot noise and the negative differential conductance can still be observed.

Finally, we note that, although the results presented here were calculated for chains of three quantum dots, similar behavior may be in principle observed for longer chains, where transport is governed by various selection rules and the current can flow due to tunneling through high-spin molecular states of the system.

Acknowledgments

We acknowledge discussions with J Barnaś. This work was supported by funds of the Polish Ministry of Science and Higher Education as a research project for the years 2008–2010, by the Alexander von Humboldt Foundation and the Foundation for Polish Science. Financial support by the Excellence Cluster 'Nanosystems Initiative Munich (NIM)' is gratefully acknowledged.

Appendix

The localized basis of quantum dot chain states is defined as $|\chi\rangle = |\chi_1\chi_2\chi_3\rangle$, where $\chi_j = 0, \uparrow, \downarrow, \mathrm{d}$ denotes zero electrons, one spin-up, spin-down electron and doubly occupied dot j. Using the $SU(2)$ symmetry for total spin one can reduce the Hilbert space from 4^3 states to 35 multiplets. The reduction of Hilbert space is important rather for analytical calculations, while in numerical calculations we have used the basis of 64 states. In the following, we give the explicit matrices for blocks of the Hamiltonian H_{chain} in the basis of total charge Q and total spin S, where to define the spin $SU(2)$ basis we have taken the highest-weight spin states. In the block $\{Q = 2, S = 0\}$, the states are: $S_1^{2,0} = |\mathrm{d}00\rangle$, $S_2^{2,0} = |0\mathrm{d}0\rangle$, $S_3^{2,0} = |00\mathrm{d}\rangle$, $S_{12}^{2,0} = \frac{1}{\sqrt{2}}(|\uparrow\downarrow 0\rangle - |\downarrow\uparrow 0\rangle)$, $S_{23}^{2,0} = \frac{1}{\sqrt{2}}(|0\uparrow\downarrow\rangle - |0\downarrow\uparrow\rangle)$ and $S_{13}^{2,0} = \frac{1}{\sqrt{2}}(|\uparrow 0\downarrow\rangle - |\downarrow 0\uparrow\rangle)$, respectively. The Hamiltonian block in this basis is given by

$$H_{2,0} = \begin{pmatrix} \varepsilon_{21} & 0 & 0 & \sqrt{2}t & 0 & 0 \\ 0 & \varepsilon_{21} & 0 & \sqrt{2}t & \sqrt{2}t & 0 \\ 0 & 0 & \varepsilon_{21} & 0 & \sqrt{2}t & 0 \\ \sqrt{2}t & \sqrt{2}t & 0 & \varepsilon_{22} & 0 & t \\ 0 & \sqrt{2}t & \sqrt{2}t & 0 & \varepsilon_{22} & t \\ 0 & 0 & 0 & t & t & \varepsilon_{23} \end{pmatrix}, \quad \text{(A.1)}$$

where $\varepsilon_{21} = 2\varepsilon + U$, $\varepsilon_{22} = 2\varepsilon + U'$ and $\varepsilon_{23} = 2\varepsilon$. The block of H_{chain} for $\{Q = 4, S = 0\}$, $H_{4,0}$, has a similar structure to $H_{2,0}$ due to particle–hole symmetry:

$$H_{4,0} = \begin{pmatrix} \varepsilon_{41} & 0 & 0 & \sqrt{2}t & 0 & 0 \\ 0 & \varepsilon_{41} - 4U' & 0 & \sqrt{2}t & \sqrt{2}t & 0 \\ 0 & 0 & \varepsilon_{41} & 0 & \sqrt{2}t & 0 \\ \sqrt{2}t & \sqrt{2}t & 0 & \varepsilon_{42} & 0 & -t \\ 0 & \sqrt{2}t & \sqrt{2}t & 0 & \varepsilon_{42} & -t \\ 0 & 0 & 0 & -t & -t & \varepsilon_{43} \end{pmatrix}, \quad \text{(A.2)}$$

where $\varepsilon_{41} = 4\varepsilon + 2U + 4U'$, $\varepsilon_{42} = 4\varepsilon + U + 3U'$ and $\varepsilon_{43} = 4\varepsilon + U + 4U'$. The states in block $\{Q = 4, S = 0\}$ are explicitly given by: $S_1^{4,0} = |0\mathrm{dd}\rangle$, $S_2^{4,0} = |\mathrm{d}0\mathrm{d}\rangle$, $S_3^{4,0} = |\mathrm{dd}0\rangle$, $S_{12}^{4,0} = \frac{1}{\sqrt{2}}(|\uparrow\downarrow\mathrm{d}\rangle - |\downarrow\uparrow\mathrm{d}\rangle)$, $S_{23}^{4,0} = \frac{1}{\sqrt{2}}(|\mathrm{d}\uparrow\downarrow\rangle - |\mathrm{d}\downarrow\uparrow\rangle)$ and $S_{13}^{4,0} = \frac{1}{\sqrt{2}}(|\uparrow\mathrm{d}\downarrow\rangle - |\downarrow\mathrm{d}\uparrow\rangle)$, respectively. On the other hand, the Hamiltonian block for $\{Q = 3, S = \frac{1}{2}\}$ is the largest one, with the states defined as follows: $D_1^{3,\frac{1}{2}} = |\mathrm{d}\uparrow 0\rangle$, $D_2^{3,\frac{1}{2}} = |0\uparrow\mathrm{d}\rangle$, $D_3^{3,\frac{1}{2}} = |\uparrow\mathrm{d}0\rangle$, $D_4^{3,\frac{1}{2}} = |0\mathrm{d}\uparrow\rangle$, $D_5^{3,\frac{1}{2}} = |\uparrow 0\mathrm{d}\rangle$, $D_6^{3,\frac{1}{2}} = |\mathrm{d}0\uparrow\rangle$, $D_7^{3,\frac{1}{2}} = \frac{1}{\sqrt{2}}(|\uparrow\downarrow\uparrow\rangle - |\downarrow\uparrow\uparrow\rangle)$ and $D_8^{3,\frac{1}{2}} = \sqrt{\frac{2}{3}}|\uparrow\uparrow\downarrow\rangle - \frac{1}{\sqrt{6}}(|\uparrow\downarrow\uparrow\rangle + |\downarrow\uparrow\uparrow\rangle)$, respectively. The block $H_{3,\frac{1}{2}}$ is explicitly given by

$$H_{3,\frac{1}{2}} = \begin{pmatrix} \varepsilon_{31} & 0 & -t & 0 & 0 & t & 0 & 0 \\ 0 & \varepsilon_{31} & 0 & -t & t & 0 & 0 & 0 \\ -t & 0 & \varepsilon_{31} & 0 & 0 & 0 & \frac{-t}{\sqrt{2}} & \sqrt{\frac{3}{2}}t \\ 0 & -t & 0 & \varepsilon_{31} & 0 & 0 & \sqrt{2}t & 0 \\ 0 & t & 0 & 0 & \varepsilon_{32} & 0 & \frac{-t}{\sqrt{2}} & \sqrt{\frac{3}{2}}t \\ t & 0 & 0 & 0 & 0 & \varepsilon_{32} & \sqrt{2}t & 0 \\ 0 & 0 & \frac{-t}{\sqrt{2}} & \sqrt{2}t & \frac{-t}{\sqrt{2}} & \sqrt{2}t & \varepsilon_{33} & 0 \\ 0 & 0 & \sqrt{\frac{3}{2}}t & 0 & \sqrt{\frac{3}{2}}t & 0 & 0 & \varepsilon_{33} \end{pmatrix}, \quad \text{(A.3)}$$

where $\varepsilon_{31} = 3\varepsilon + U + 2U'$, $\varepsilon_{32} = 3\varepsilon + U$ and $\varepsilon_{33} = 3\varepsilon + 2U'$. For completeness, we also give the matrices for smaller blocks of the Hamiltonian:

$$H_{1,\frac{1}{2}} = \begin{pmatrix} \varepsilon & t & 0 \\ t & \varepsilon & t \\ 0 & t & \varepsilon \end{pmatrix}, \quad \text{(A.4)}$$

$$H_{2,1} = \begin{pmatrix} 2\varepsilon + U' & t & 0 \\ t & 2\varepsilon & t \\ 0 & t & 2\varepsilon + U' \end{pmatrix}. \quad \text{(A.5)}$$

The states for block $\{Q = 1, S = \frac{1}{2}\}$ are: $D_1^{1,\frac{1}{2}} = |\uparrow 00\rangle$, $D_2^{1,\frac{1}{2}} = |0\uparrow 0\rangle$ and $D_3^{1,\frac{1}{2}} = |00\uparrow\rangle$, while for block $\{Q = 2, S = 1\}$ they are given by: $T_1^{1,1} = |\uparrow\uparrow 0\rangle$, $T_2^{1,1} = |\uparrow 0\uparrow\rangle$ and $T_3^{1,1} = |0\uparrow\uparrow\rangle$, respectively. The Hamiltonian blocks $H_{5,\frac{1}{2}}$ and $H_{4,1}$ have similar structure to blocks $H_{1,\frac{1}{2}}$ and $H_{2,1}$ due to particle–hole symmetry. On the other hand, blocks $H_{0,0}$, $H_{3,\frac{3}{2}}$ and $H_{6,0}$ are trivially one-dimensional, see also table 1.

References

[1] Julliere M 1975 *Phys. Lett.* A **54** 225
[2] Barnaś J and Fert A 1998 *Phys. Rev. Lett.* **80** 1058
Takahashi S and Maekawa S 1998 *Phys. Rev. Lett.* **80** 1758
[3] Bułka B R 2000 *Phys. Rev.* B **62** 1186
[4] Rudziński W and Barnaś J 2001 *Phys. Rev.* B **64** 085318
[5] König J and Martinek J 2003 *Phys. Rev. Lett.* **90** 166602
[6] Braun M, König J and Martinek J 2004 *Phys. Rev.* B **70** 195345
Braun M, König J and Martinek J 2006 *Phys. Rev.* B **74** 075328
[7] Weymann I, König J, Martinek J, Barnaś J and Schön G 2005 *Phys. Rev.* B **72** 115334
[8] Braig S and Brouwer P W 2005 *Phys. Rev.* B **71** 195324
[9] Weymann I and Barnaś J 2006 *Phys. Rev.* B **73** 205309

Weymann I and Barnaś J 2007 *Phys. Rev.* B **75** 155308
Weymann I and Barnaś J 2008 *Phys. Rev.* B **77** 075305
[10] Souza F M, Egues J C and Jauho A P 2007 *Phys. Rev.* B **75** 165303
[11] Fransson J 2005 *Europhys. Lett.* **70** 796
[12] Cottet A, Belzig W and Bruder C 2004 *Phys. Rev.* B **70** 115315
Cottet A, Belzig W and Bruder C 2004 *Phys. Rev. Lett.* **92** 206801
Cottet A and Choi M-S 2006 *Phys. Rev.* B **74** 235316
[13] Martinek J, Utsumi Y, Imamura H, Barnaś J, Maekawa S, König J and Schön G 2003 *Phys. Rev. Lett.* **91** 127203
Choi M-S, Sanchez D and Lopez R 2004 *Phys. Rev. Lett.* **92** 056601
[14] Sindel M, Borda L, Martinek J, Bulla R, König J, Schön G, Maekawa S and von Delft J 2007 *Phys. Rev.* B **76** 045321
[15] Weymann I 2008 *Phys. Rev.* B **78** 045310
[16] Barnaś J and Weymann I 2008 *J. Phys.: Condens. Matter* **20** 423202
[17] Wolf S A, Awschalom D D, Buhrman R A, Daughton J M, von Molnar S, Roukes M L, Chtchelka A Y and Treger D M 2001 *Science* **294** 1488
[18] Awschalom D D, Loss D and Samarth N 2002 *Semiconductor Spintronics and Quantum Computation* (Berlin: Springer)
[19] Maekawa S and Shinjo T 2002 *Spin Dependent Transport in Magnetic Nanostructures* (New York: Taylor and Francis)
[20] Zutic I, Fabian J and Das Sarma S 2004 *Rev. Mod. Phys.* **76** 323
[21] Loss D and DiVincenzo D P 1998 *Phys. Rev.* A **57** 120
[22] Zhao B, Mönch I, Vinzelberg H, Mühl T and Schneider C M 2002 *Appl. Phys. Lett.* **80** 3144
Zhao B, Mönch I, Vinzelberg H, Mühl T and Schneider C M 2002 *J. Appl. Phys.* **91** 7026
[23] Jensen A, Hauptmann J R, Nygard J and Lindelof P E 2005 *Phys. Rev.* B **72** 035419
[24] Sahoo S, Kontos T, Furer J, Hoffmann C, Gräber M, Cottet A and Schönenberger C 2005 *Nat. Phys.* **1** 102
[25] Pasupathy A N, Bialczak R C, Martinek J, Grose J E, Donev L A K, McEuen P L and Ralph D C 2004 *Science* **306** 86
[26] Bernand-Mantel A, Seneor P, Lidgi N, Munoz M, Cros V, Fusil S, Bouzehouane K, Deranlot C, Vaures A, Petroff F and Fert A 2006 *Appl. Phys. Lett.* **89** 062502
[27] Hamaya K, Masubuchi S, Kawamura M, Machida T, Jung M, Shibata K, Hirakawa K, Taniyama T, Ishida S and Arakawa Y 2007 *Appl. Phys. Lett.* **90** 053108
[28] Hamaya K, Kitabatake M, Shibata K, Jung M, Kawamura M, Hirakawa K, Machida T, Taniyama T, Ishida S and Arakawa Y 2007 *Appl. Phys. Lett.* **91** 22107
Hamaya K, Kitabatake M, Shibata K, Jung M, Kawamura M, Hirakawa K, Machida T, Taniyama T, Ishida S and Arakawa Y 2007 *Appl. Phys. Lett.* **91** 232105
[29] Hamaya K, Kitabatake M, Shibata K, Jung M, Kawamura M, Ishida S, Taniyama T, Hirakawa K, Arakawa Y and Machida T 2008 *Phys. Rev.* B **77** 081302(R)
[30] Yang H, Yang S-H and Parkin S S P 2008 *Nano Lett.* **8** 340
[31] Hauptmann J R, Paaske J and Lindelof P E 2008 *Nat. Phys.* **4** 373
[32] Saraga D S and Loss D 2003 *Phys. Rev. Lett.* **90** 166803
[33] Jiang Z-T, Sun Q-F and Wang Y 2005 *Phys. Rev.* B **72** 045332
[34] de Guevara M R L and Orellana P A 2006 *Phys. Rev.* B **73** 205303
[35] Aghassi J, Thielmann A, Hettler M H and Schön G 2006 *Appl. Phys. Lett.* **89** 052101
[36] Kuzmenko T, Kikoin K and Avishai Y 2006 *Phys. Rev. Lett.* **96** 046601
Kuzmenko T, Kikoin K and Avishai Y 2006 *Phys. Rev.* B **73** 235310
[37] Emary C 2007 *Phys. Rev.* B **76** 245319
[38] Delgado F, Shim Y-P, Korkusinski M and Hawrylak P 2007 *Phys. Rev.* B **76** 115332
[39] Trocha P and Barnaś J 2008 *Phys. Rev.* B **78** 075424
[40] Vernek E, Büsser C A, Martins G B, Anda E V, Sandler N and Ulloa S E 2009 arXiv:0902.2926v1
[41] Kostyrko T and Bułka B R 2009 *Phys. Rev.* B **79** 075310
[42] Waugh F R, Berry M J, Mar D J, Westervelt R M, Campman K L and Gossard A C 1995 *Phys. Rev. Lett.* **75** 705
[43] Gaudreau L, Studenikin S A, Sachrajda A S, Zawadzki P, Kam A, Lapointe J, Korkusinski M and Hawrylak P 2006 *Phys. Rev. Lett.* **97** 036807
[44] Schröer D, Greentree A D, Gaudreau L, Eberl K, Hollenberg L C L, Kotthaus J P and Ludwig S 2007 *Phys. Rev.* B **76** 075306
[45] Chen Yu and Goldman A M 2007 *Appl. Phys. Lett.* **91** 063119
[46] Grove-Rasmussen K, Jørgensen H I, Hayashi T, Lindelof P E and Fujisawa T 2008 arXiv:0804.3441v1
[47] Rogge M C and Haug R J 2008 *Phys. Rev.* B **77** 193306
[48] Peres N M R, Stauber T and Lopes dos Santos J M B 2009 *Phys. Rev.* B **79** 035107
[49] Kim J, Melnikov D V and Leburton J-P 2009 *Phys. Rev.* B **80** 045305
[50] Gaudreau L, Sachrajda A S, Studenikin S, Kam A, Delgado F, Shim Y P, Korkusinski M and Hawrylak P 2009 *Phys. Rev.* B **80** 075415
[51] Trocha P and Barnaś J 2008 *J. Phys.: Condens. Matter* **20** 125220
[52] Schoeller H and Schön G 1994 *Phys. Rev.* B **50** 18436
König J, Schmid J, Schoeller H and Schön G 1996 *Phys. Rev.* B **54** 16820
König J 1999 *Quantum Fluctuations in the Single-Electron Transistor* (Aachen: Shaker)
[53] Thielmann A, Hettler M H, König J and Schön G 2005 *Phys. Rev. Lett.* **95** 146806
[54] Grabert H and Devoret M H 1992 *Single Charge Tunneling: Coulomb Blockade Phenomena in Nanostructures* (*NATO ASI Series B: Physics* 294) (New York: Plenum)
[55] Averin D V and Odintsov A A 1989 *Phys. Lett.* A **140** 251
Averin D V and Nazarov Yu V 1990 *Phys. Rev. Lett.* **65** 2446
Kang K and Min B I 1997 *Phys. Rev.* B **55** 15412
[56] Blanter Ya M and Büttiker M 2000 *Phys. Rep.* **336** 1
[57] Simmons C B, Thalakulam Madhu, Rosemeyer B M, Van Bael B J, Sackmann E K, Savage D E, Lagally M G, Joynt R, Friesen M, Coppersmith S N and Eriksson M A 2009 *Nano Lett.* **9** 3234
[58] Sukhorukov E V, Burkard G and Loss D 2001 *Phys. Rev.* B **63** 125315
[59] Thielmann A, Hettler M H, König J and Schön G 2003 *Phys. Rev.* B **68** 115105